Hindawi
Geofluids
Volume 2022, Article ID 9113173, 14 pages
https://doi.org/10.1155/2022/9113173

Research Article

Stability Analysis of a Steep Rock Slope in a Large Open-Pit Mine in a High-Intensity Area: A Case Study of the Yejiagou Boron Iron Mine

Ying Zhang,[1,2,3] Jiabing Zhang,[2,4] and Junhua Ma[1,3]

[1]*Liaoning Nonferrous Geological Exploration and Research Institute Co., Shenyang 110013, China*
[2]*College of Construction Engineering, Jilin University, Changchun 130026, China*
[3]*Technology Innovation Center for Old Mine Geological Disaster Prevention and Ecological Restoration, Ministry of Natural Resources, Shenyang 110013, China*
[4]*College of Civil Engineering and Architecture, Xinjiang University, Urumqi 830046, China*

Correspondence should be addressed to Jiabing Zhang; zhangjiabing@stu.xju.edu.cn

Received 18 May 2022; Revised 18 June 2022; Accepted 28 June 2022; Published 18 August 2022

Academic Editor: Zhenlong Song

The slope stability of open-pit mines has always been a major problem affecting the safe production of resources from open-pit step mines. At present, slope excavation in open-pit mines is difficult and slope instability problems are becoming increasingly prominent. In this study, an open-pit bench rock slope in Liaoning Province was taken as the research object. The physical parameters of the rock mass in the area were obtained through engineering drilling and large-scale direct shear tests. Based on the determination of the dominant group of the slope's structural plane, the seepage deformation failure and maximum stress deformation of the slope were analyzed to explore the stability of high and steep rocky slopes in large open-pit mines. The results show that there is a group of dominant structural planes at the no. 1~3 observation points whose dip angle is steep and consistent with the slope inclination. The dip angle is slightly lesser at the slope toe, and the slope is basically a stable structure. The Janbu method was used to calculate the seepage stability of the slope and it is found that section 4-4 is in a dangerous area. In the stress nephogram, the maximum principal stress is located inside the slope, and the minimum principal stress is located at the surface of the free surface.

1. Introduction

Open-pit mining is an important mining type in China. With the decrease in shallow mineral resources, the depth of open-pit mining has gradually increased, the height of the slopes has continuously increased, and slope stability problems have become increasingly more prominent [1–9]. Wu et al. [10] established the Flac^{3D} slope model and developed a statistical mechanics of rock masses (SMRM) calculation system based on statistical mechanics data of rock masses. This system can provide a fast and accurate solution for the estimation of the elastic modulus, Poisson's ratio, shear strength, and other parameters. Cambio et al. [11] inversed and calibrated the strength parameters of a rock mass and its structural characteristics. The strength parameters of the rock mass and its structural characteristics were inversely analyzed and calibrated. At the same time, FLAC^{3D} has been used to establish a numerical model of a slope in the open-pit mine in Bingham Valley and analyze the conditions and trigger factors of slope movement. Yang et al. [12] explored the deformation mode of a high and steep layered rock slope and its failure mechanism caused by gradual excavation; FLAC^{3D} was used to simulate the excavation process according to the actual situation. Srikrishnan et al. [13] simulated an open-pit slope composed of different rock types using FLAC^{3D}.

Chen and Zhang [14] studied the compression response of space variable rock columns with three-dimensional random fields. Cao et al. [15, 16] studied the settlement and deformation of an open-pit mine dump by combining field

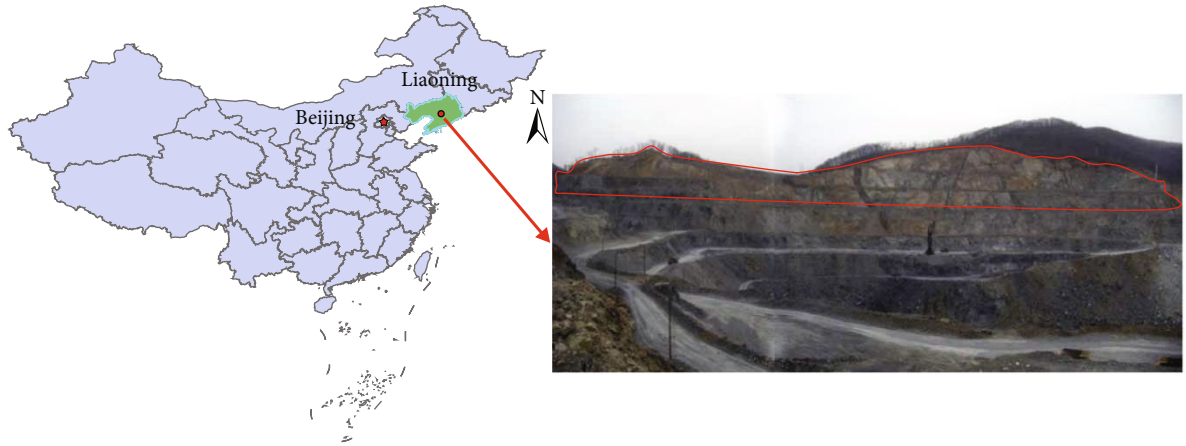

Figure 1: Rock slope panorama.

monitoring data and numerical simulations. Zhang et al. [17] analyzed the anchor cable monitoring in the Nanfen open-pit mine and revealed the failure process of a bedding rock landslide and the stress evolution characteristics of negative Poisson's ratio (NPR) cables. Xu and Yan [18] used FLAC^{3D} to simulate the influence of excavation and blasting vibration on goaf stability. Li et al. [19] analyzed the failure process of a steeply inclined layered carbonate rock slope induced by the presence of an underground goaf. Tao et al. [20] established a three-dimensional model of the slope on an entire mine slope using FLAC^{3D} and calculated the slope stability using 3DEC. Zhu et al. [21] used FLAC^{3D} to simulate the anchorage mechanism of a layered rock mass with different numbers of bolts. Liang et al. [22] used the BP neural network algorithm to establish a stable slope angle prediction model of an open-pit mine and successfully predicted the final slope angle of the mine. Gong et al. [23, 24] analyzed the impact of rainfall on open-pit coal mines.

At present, many scholars have studied the deformation mechanism of open-pit mine slopes, and their results are valuable to ensure the safe mining of slopes [25–31]. In this paper, the rock slope of an open-pit mine is taken as the research object. The physical parameters of each rock layer are obtained using field geological exploration, engineering drilling geophysical exploration, and large direct shear experiments. GEOSLOPE is used to analyze the seepage deformation and failure of slope, and FLAC^{3D} is used to carry out a three-dimensional numerical simulation of the slope. The results of this study serve as a scientific basis for safe operations in the mining area.

2. Project Overview

The rock slope of the open-pit mine is located in Fengcheng City, Liaoning Province (Figure 1). The overall distribution of slope is along the east and west direction. The highest point of the slope's elevation is about 570 m, and the lowest point is about 430 m. The overall slope trends about 140°-210° southward, and the slope angle is about 66°. The terrain is high in the east and low in the west, and the multistage steps are sloped, with a step height of about 20 m.

Table 1: Dominant grouping of joint fissures at the observation points.

Observation point number	Number of groups	Number	Average propensity (°)	Average dip angle (°)
1	1	13	4	60
	2	7	210	54
	3	10	91	72
2	1	16	340	66
	2	15	194	55
	3	6	55	60
	4	3	305	77
3	1	45	347	66
	2	25	244	77
	3	12	74	30
4	1	17	342	65
	2	20	94	35
	3	7	84	82
	4	4	267	73

The lithology of the rock slope is simple. It is mainly composed of biotite granulite (metamorphic rock series) of the Lieryu Formation of the middle and lower Proterozoic Liaohe Group. It is mainly composed of serpentine and granulite. The ore body is mainly composed of calcium magnesium and iron magnesium silicate rock and magnesium-rich carbonate rock. It is mainly composed of iron borosite and phosphorite, accompanied by radioactive elements and rare earth elements. The thickness of slope varies significantly.

The mining area is located in the middle of Jiaoliaotai Longyingkou and stretches to the Kuandiantai arch. With the development of multistage metamorphic deformation, the migmatization is strong, and rock joints and fissures are developed. The slope's rock mass is seriously broken due to the overall influence of blasting in the open-pit mine. Due to the drilling exposure, drilling holes in the slope have

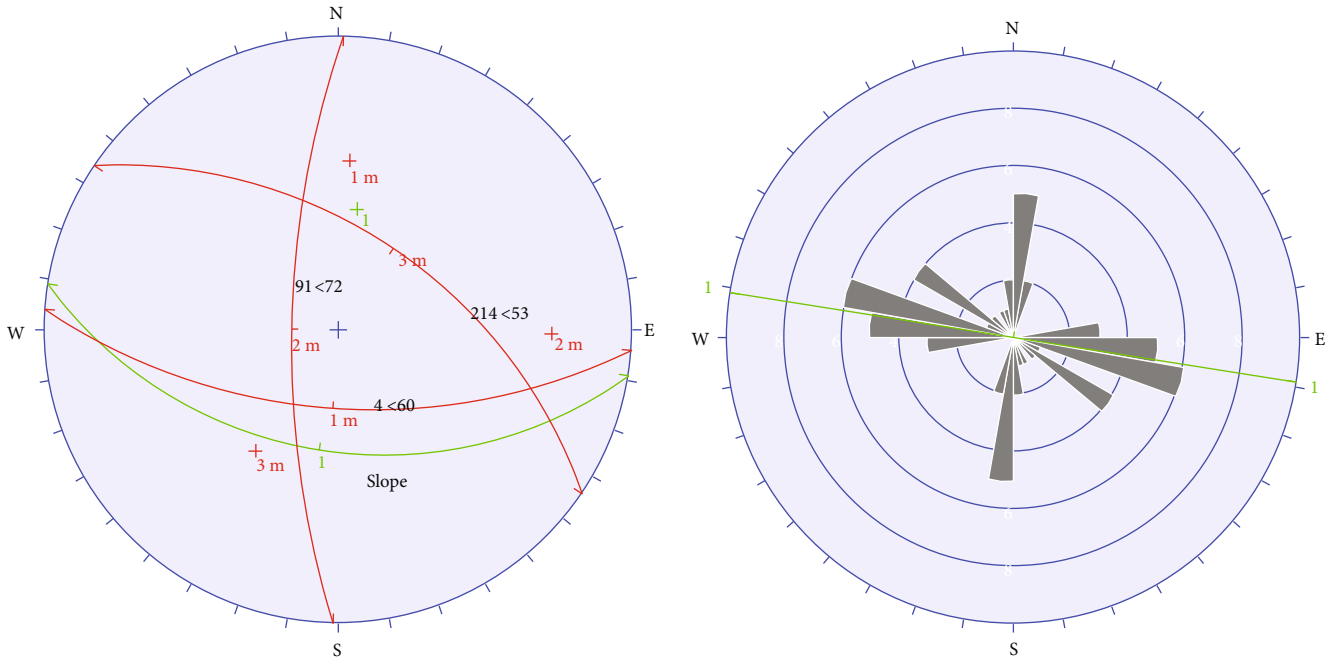

Figure 2: No. 1 observation point stereographic projection and joint rose map.

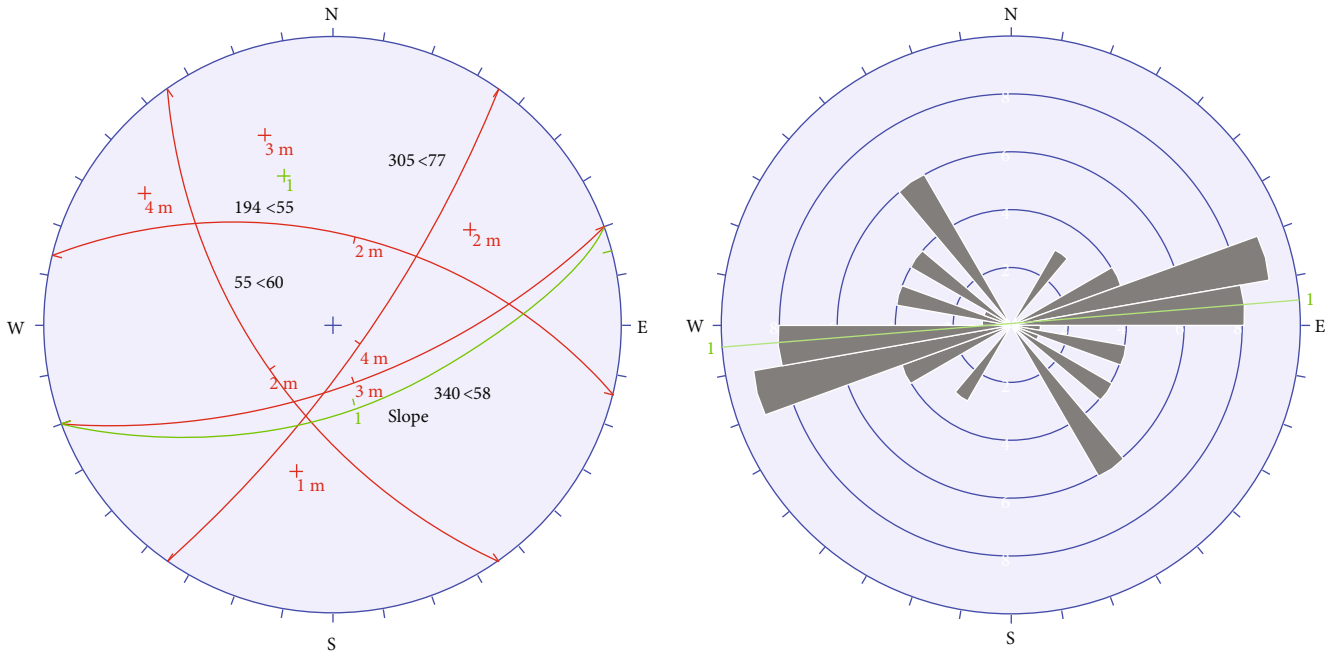

Figure 3: No. 2 observation point stereographic projection and joint rose map.

integrity till a depth of 25 m and then the hole is extremely broken; the core is composed of gravel and broken blocks.

3. Slope Deformation and Failure

3.1. Dominant Grouping of the Slope's Structural Plane. To comprehensively study the slope surface, joint fissures, and their combination and explore the potential deformation and failure mode of the slope, four observation points (nos. 1-4) were set to measure the slope joint fissures and slope occurrence (Table 1). A total of 200 groups of inclinations and dip angles were counted, and a polar stereographic projection map and joint rose map of each observation point were plotted. Then, the dominant structural plane grouping

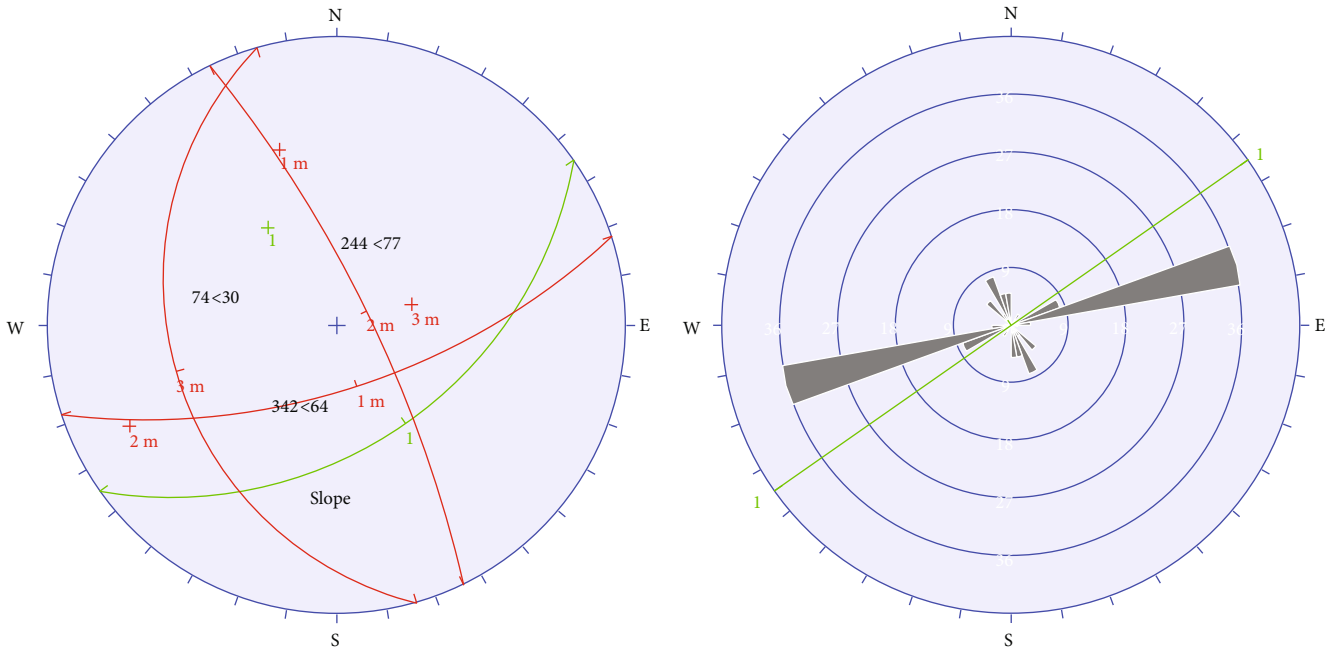

Figure 4: No. 3 observation point stereographic projection and joint rose map.

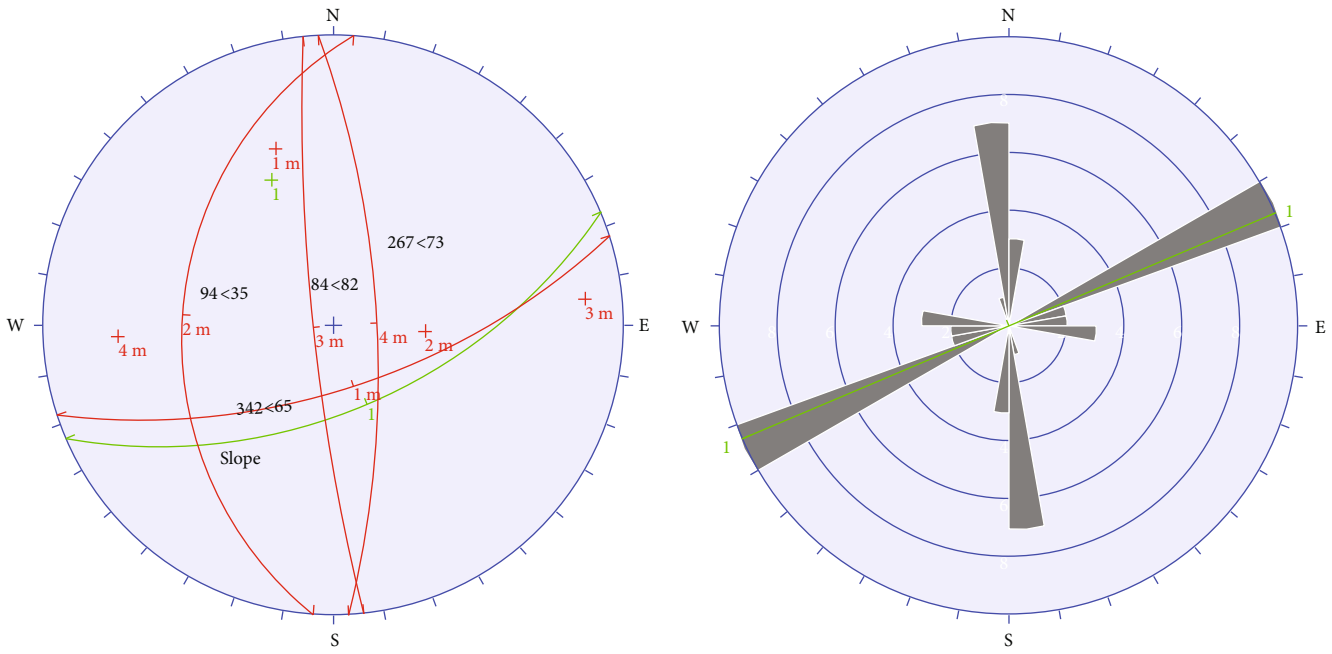

Figure 5: No. 4 observation point stereographic projection and joint rose map.

of each observation point was obtained to determine the joint fracture development of the slope, as shown in Figures 2–5.

There is a group of dominant structural planes at observation points 1~3, which are consistent with the slope inclination. The slope has a steep inclination which is smaller than the angle at the slope toe. There is a group of dominant structural planes with the same inclination as the slope at observation point 4. The intersection of the inclination of the two groups of structural planes is consistent with the slope inclination. The included angle between the intersection inclination of the structural plane and the slope inclination is less than 45°, and the intersection inclination is less than the slope inclination, but the intersection inclination angle is 10.3°, which is less than the joint fissure friction angle of 16.3°. Here, the slope basically has a stable structure.

3.2. Slope Deformation and Failure. Field investigations of the slope show that the deformation is mainly unloading rebound. Before the slope is formed, a certain amount of

Figure 6: Deformation and failure diagram of the slope.

deformation energy is accumulated due to the influence of in situ stress. After the slope is formed, the deformation energy of the rock mass near the slope is released under the unloading action of the free face, resulting in the deformation of the slope. Due to the formation of the rebound load, the greater the original residual structural stress, the greater the rebound deformation of the free face. When the deformation exceeds the limit state, a tensile fracture surface is generated. The field investigations revealed an unloading tension crack with a strike of 120°, a length of about 15 m, a maximum width of 5 cm, and a maximum depth of about 0.5 m with no sliding at the rear edge of the slope. At the 454 m step on the south side of the slope, there are many tensile cracks near the edge, of which the largest crack is about 40 cm wide, 15 cm narrow, and 60 cm long as shown in Figure 6.

The failure modes of the boundary slope within the scope of this survey mainly include plane sliding, circular arc failure, toppling failure, collapse failure, and so on:

(1) Plane sliding: it is characterized by the development of a group of discontinuous structural planes with a strike parallel to the slope, a tendency consistent with the slope tendency, and a dip angle that is less than or close to the slope angle in the slope's rock mass. When the slope's rock mass slides along the structural plane, it undergoes plane failure. According to the statistics from the joint fissure observation points, there is a group of joint surfaces with a strike parallel to the slope and a tendency consistent with the slope inclination in each slope section of the survey slope. The dip angle is slightly steeper than the slope angle, and the difference between the dip angle of the structural plane and the slope angle is only about 5°. However, when the slope excavated by mining is steep or there is an overbreak-free surface and these are combined with weathering, the strength of the rock mass is reduced and the impact of engineering activities such as blasting will affect the slope and make it prone to plane failure

(2) Circular arc failure: when the rock mass of the slope is in a broken to extremely broken state and the rock mass is in a loose structure or cataclastic structure, circular arc failure may occur. Under the influence of blasting and mining activities, the rock mass at the slope steps in this survey is generally broken~extremely broken at a depth of 20-25 m and locally within 30 m, and circular arc sliding failure may occur in the broken~extremely broken hill

(3) Toppling failure: when a steeply dipping joint plane or schistosity plane is developed in a rock mass with a massive structure and there is a free slope surface parallel to the structural plane, the slope's rock mass can gradually deform and topple along the discontinuous surface. Generally, the scale is not large, and most of them are of the bench slope failure type. According to the statistics of the joint fissures, there is a group of steeply dipping joint surfaces with a tendency basically consistent with that of the slope

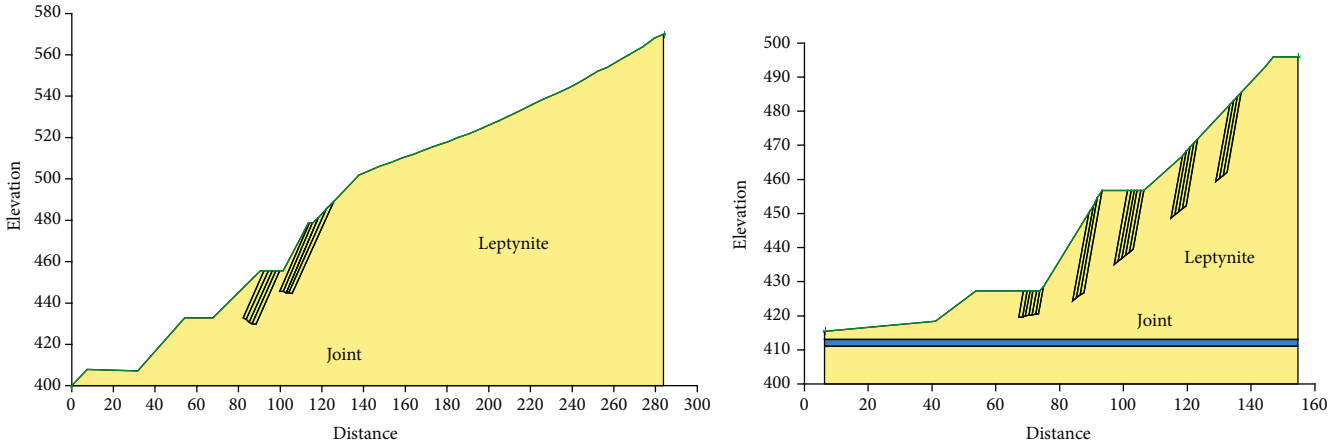

Figure 7: Section 1-1 and section 4-4 model diagram.

in this survey, especially the slope at section 3 and section 4. In the section with the steep slope angle, the slope rock mass has been overturned and the scale is small, showing bench slope failure. If the slope toe is enlarged, a free face will be formed, which will gradually deform and dump the slope's rock mass along the discontinuous surface, resulting in dumping failure of the slope's rock mass

(4) Collapse failure: in steep slopes and slope sections, collapse occurs easily when joints and fissures are developed and the rock mass is broken. When the positions of the various weak structural planes in a rock mass are in the most unfavorable locations, collapse also occurs easily. In addition, the change in temperature between day and night and the change in the seasonal temperature also promote rock weathering, the scouring of surface water, and the dissolution and softening of fissure fillings to form a weak surface. Also, the infiltration of water increases the hydrostatic pressure, and earthquakes, mine blasting, and too high slope excavation destroy the mountain slopes' balance, which all promote the occurrence of collapse

The statistics of the joints and fissures show that there are many groups of very well-developed conjugate joints in the surveyed slope. In addition, the slope is affected by mining activities, resulting in the fragmentation of the slope's rock mass and making the slope easily prone to failure.

4. Slope Seepage Stability Analysis

The surface and groundwater of slope are important factors causing slope instability. Rainwater also penetrates into the slope joints to increase the water saturation of the slope's rock and soil mass. This reduces the substrate suction of the unsaturated area and thus reduces the shear strength of the rock mass. Slope instability occurs when the intensity and time of rainfall exceed a certain range. Similarly, the level of groundwater directly affects the stability of the slope,

Table 2: Calculation parameters of the slope seepage stability.

Rock-soil mass	Unit weight γ (kN/m^3)	Shear strength parameters	
		Cohesion (kPa)	Angle of internal friction φ (°)
Leptynite	26.4	200	35.0
Joint fissure surface	26.0	17.5	16.3

and with the rise and fall of the water level, the shear strength index of the rock mass changes.

Field investigations show that the rock and soil properties of slope are complex, and the rock and soil medium is mainly composed of variable granular rock with joint and fissure development and good permeability. Based on the analysis of the slope deformation and failure mode, the Janbu method in the GEOSLOPE software was used to analyze the slope seepage stability (Figure 7). The stability calculation was carried out considering 1-3 working conditions: working condition 1—dead weight, without considering the action of water; working condition 2—dead weight +seepage, considering the effect of surface water and groundwater seepage; and working condition 3—dead weight+seepage+earthquake. For working condition 2, seismic action is considered. The parameters related to the stability calculation are shown in Table 2.

Section 1-1 is located on the east side of the slope. The stratum is a metamorphic rock, joint fracture surfaces are developed, and there are groups of joints that are basically consistent with the slope inclination; however, the inclination is slightly larger than the slope angle. The possibility of sliding failure along the joint fracture surface is not large, and no groundwater was encountered during field drilling. Therefore, given the large degree of weathering of the shallow surface of the slope, the joint cracks are cut and broken, and the failure mode is sliding along the arc. The stability calculation results of the working conditions (1-3) are shown in Figure 8.

According to the circular arc sliding mode, the safety factor of the 1-1 section is greater than the minimum safety

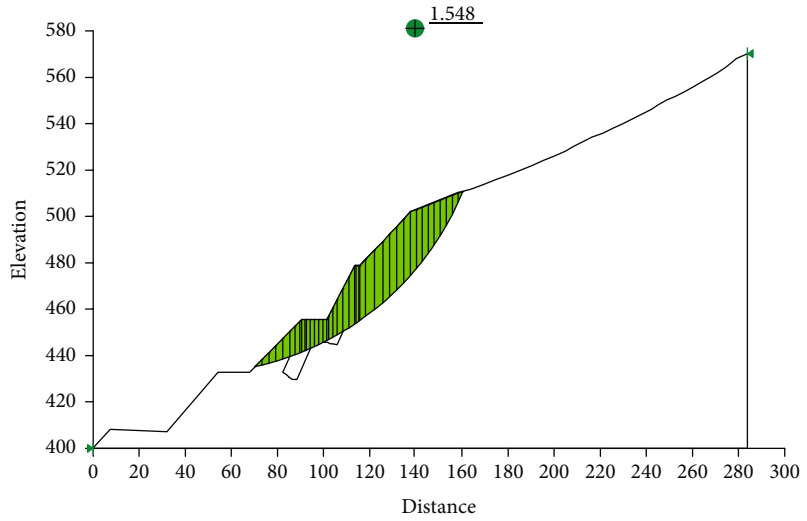

(a) Working condition 1

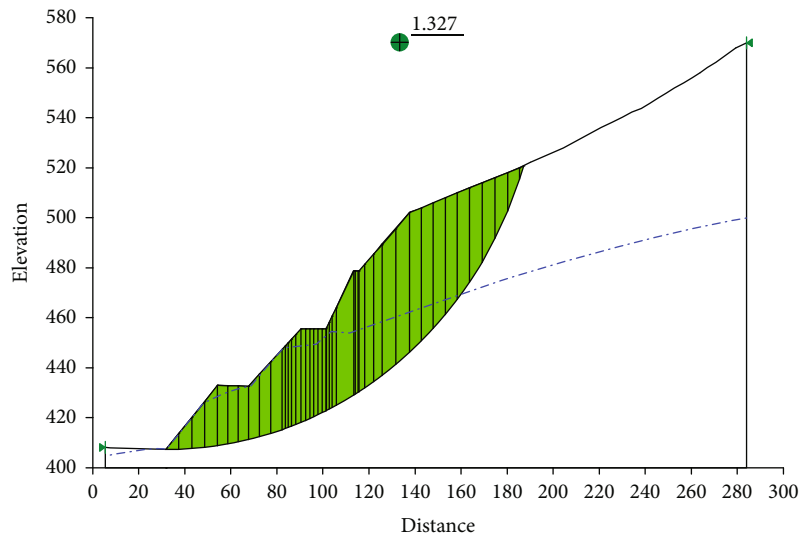

(b) Working condition 2

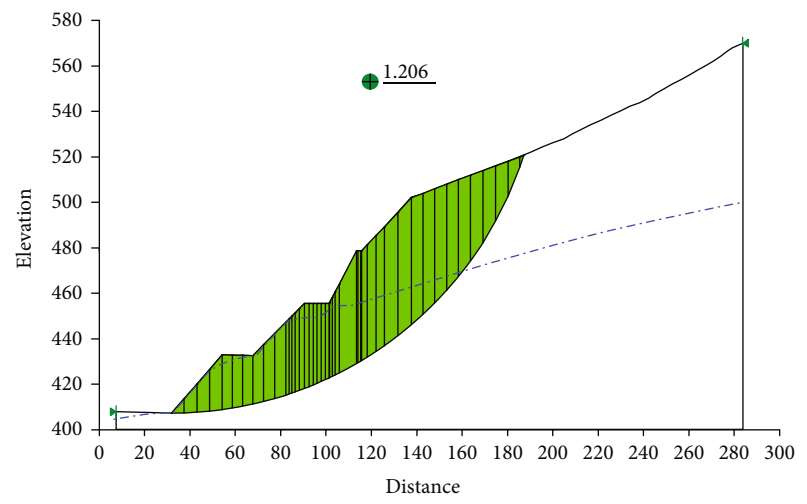

(c) Working condition 3

Figure 8: Seepage calculation diagram of section 1-1.

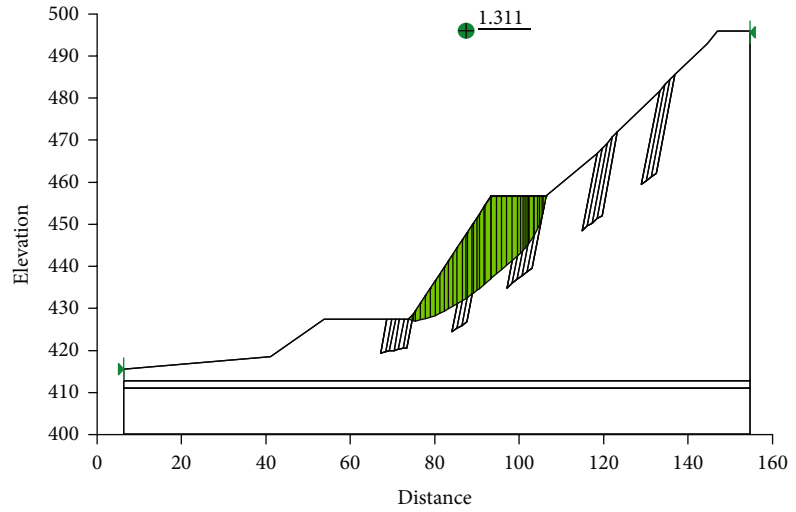

(a) Working condition 1

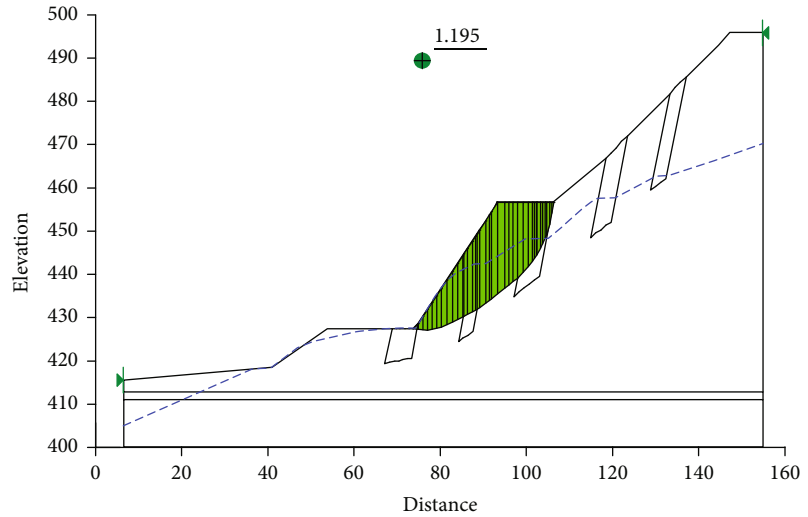

(b) Working condition 2

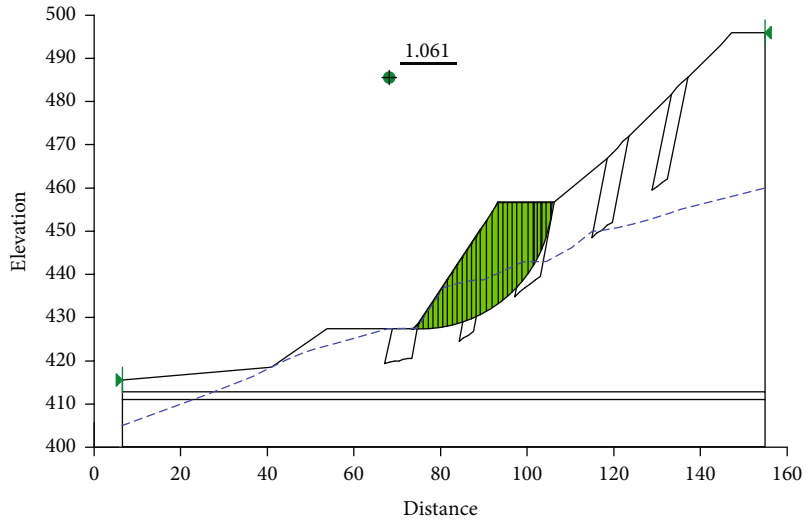

(c) Working condition 3

Figure 9: Seepage calculation diagram of section 4-4.

Table 3: Calculation results of the seepage stability of the slope sections.

Section number	Working condition	Sliding center x (m)	Sliding center y (m)	Slide-way radius (m)	Coefficient of stability	Safety factor limit
1-1 section	Working condition 1	43.004	559.363	127.12	1.548	1.30
	Working condition 2	32.07	570.179	162.877	1.327	1.15
	Working condition 3	34.06	569.4	145.56	1.206	1.10
2-2 section	Working condition 1	70.157	463.653	36.317	1.155	1.30
	Working condition 2	73.048	460.429	32.963	1.325	1.15
	Working condition 3	75.399	457.808	30.418	1.061	1.10

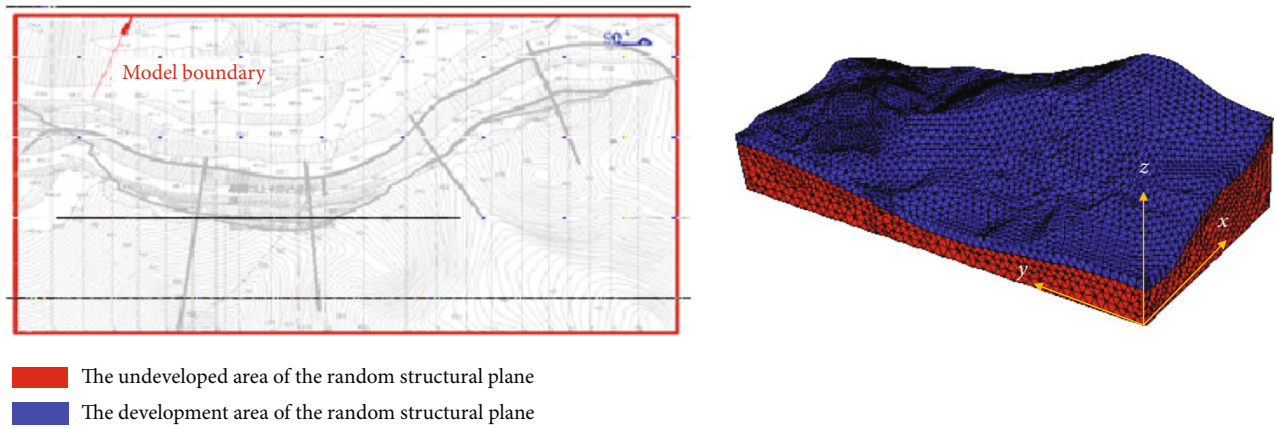

Figure 10: Schematic diagram of the 3D model and the mesh division of the slope.

factor required by the geotechnical specifications under working conditions 1, 2, and 3. On the whole, the section is in a safe state. Under the condition of rainfall seepage, the safety factor decreases slightly, indicating that rainfall infiltration can lead to the decrease in the slope's safety factor, which is an important factor in slope stability analysis when the slope is in a stable state under seismic conditions.

Section 4-4 is located in the west side of the P1 slope. The stratum is a metamorphic rock, the joint fracture surface is developed, and it has an inclined distribution that is steeper than the free surface of the slope, and it is steep cutting. Sliding along the joint fracture surface is not likely to occur. There is an excavation adit at about 410 meters, and no groundwater was encountered during field drilling. Given the large weathering degree of the shallow surface of the slope, the joint cracks are cut and broken, and the failure mode is sliding along the arc (Figure 9).

According to the circular arc sliding mode, the safety factor of the 4-4 section is greater than the safety factor required by the geotechnical specification under working conditions 1 and 2. Under working condition 3, the Janbu method was used to calculate the minimum safety factor and ensure that it was less than the specification. The section is in a dangerous area of the slope. Under the condition of seismic seepage, the local slope is in an unstable state. There is a possibility of integral step cutting and sliding failure occurring on the grading platform of the slope. Combined with the site, a steeply inclined joint fracture surface is also developed here. The adit with an elevation of 410 m has a small diameter and a low buried depth. It is preliminarily judged that it has little effect on the stability of the slope and can be plugged at the opening, but the drainage channel should still be retained (Table 3).

5. Three-Dimensional Numerical Simulation of the Slope Stability

Model establishment and parameter selection of the geological slope surface map of the slope in this 3D numerical simulation are carried out by using ANSYS and FLAC^{3D} software together. The size of this rocky slope model is approximately 800 m in length along the east-west direction of the slope, nearly 400 m in width from north to south, and about 250 m in height of the slope vertically. Using the data preprocessing function of ANSYS, the random structural plane development area above the weathered crust on the surface of the bedrock was divided into triangular tetrahedral units, with a total of 11061 nodes and 56940 units. Horizontal constraints were imposed on both sides (X and Y directions) of the model, and vertical constraints were imposed on the bottom (Z direction). The Mohr-Coulomb constitutive model was adopted as shown in Figure 10.

According to the survey data, the lithology of the slope is composed of leptynite. Therefore, according to the development degree of the random structural plane of the rock and the integrity division of the rock, the slope is divided into two layers based on the influence of the random structural plane on the stability. Taking 25 m from the bottom of the

Table 4: Parameters of the rock slope model.

Name	Density (g/cm^3)	Poisson's ratio	Elastic modulus (MPa)	Volume modulus (MPa)	Shear modulus (MPa)	Friction angle (°)	Cohesion (KPa)	Tensile strength (MPa)
Random structural plane undeveloped leptynite	2.64	0.24	40000	25640	16130	35.00	200	4.9
Random structural plane developed leptynite	2.6	0.25	32000	21333	12800	32.00	120	4.0

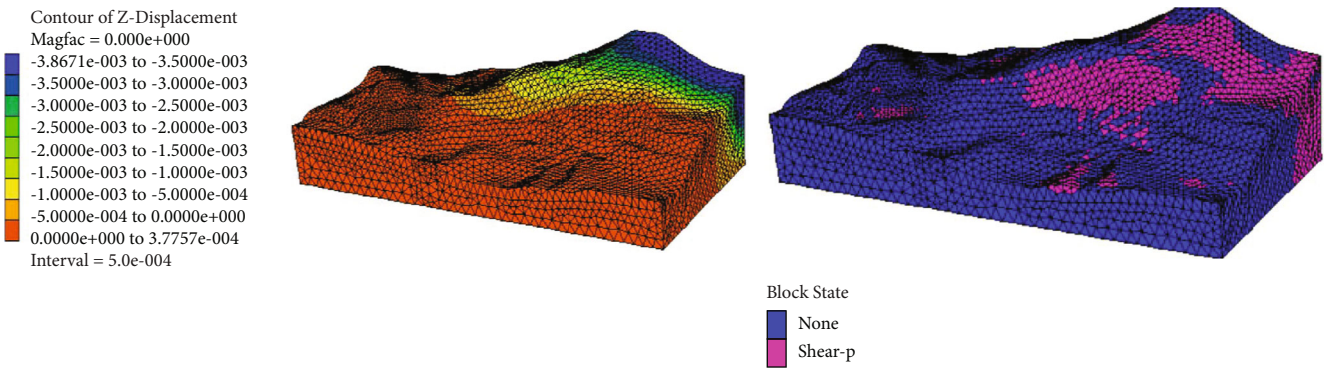

Figure 11: The cloud chart of maximum and minimum principal stress.

bedrock model as the node, the upper part is the development area of the random structural plane and the bottom part is the undeveloped area of the random structural plane. The entire slope is divided into two layers. The detailed parameters of each stratum of the rock are shown in Table 4.

In the cloud chart of the stress analysis, the maximum principal stress area is mainly the vertical self-weight stress, which is distributed in the bottom of the slope, while the minimum principal stress area corresponds to the face of the slope facing the air. Locally, due to the dense development of random structural planes, the stress is released to the air face's direction, resulting in a reverse tensile stress area, which is more consistent with the toppling tensile crack failure phenomenon formed by the development of fracture zones on the surface of the slope (Figure 11).

In the cloud chart of the stress analysis, the displacement in the X direction is greater than that in the Y direction. Under the action of the gravity of the slip zone on the surface of the air face, the displacement in the X direction is generated from the top of the north slope to the bottom of the south slope, which is consistent with the displacement movement of the slope's body in the opposite direction along the main axis. The rock at the top of the slope compresses the rock at the bottom of the slope, resulting in the fracture of the slope body, the rise of rock and soil, and the displacement in the positive X direction. The displacement in the Y direction is consistent with the movement in the positive direction of the main axis because the terrain of the slope is high in the east and low in the west. Taking the highest ridge of the terrain as the displacement change boundary, it gradually decreases to the west and the back-up part is connected with the shear stress zone. Due to the existence of tension cracks, local displacement relative to the overall y-axis direction occurs, which is also consistent with the actual situation on site. The displacement distribution in the Z direction is generally large at the top and small at the bottom. This means that the vertical displacement of the surface layer, especially at the north slope at the height of the terrain, is the maximum and gradually decreases in the downward and southward directions until it is consistent with the displacement of the surrounding rock mass and does not form a relative displacement (Figure 12).

It can be seen from the cloud chart of the plastic zone that with the development of the random structural plane on the surface of the slope, large and small shear plastic zones are formed on the surface of the slope, especially at the trailing edge of the slope, where a shear stress concentration zone is formed (Figure 13). When the shear strength of the shear zone exceeds the ultimate shear strength of the rock, the slope will become unstable. According to the current calculation results and the actual situation on-site, there is only one continuous shear zone that has not been penetrated, and this does not pose a serious threat to the stability of the slope (Figure 14).

From the perspective of the entire slope, the deformation value of the section at $X = 350$ m is large. It can be seen from the cloud chart that vertical displacement occurs in the z-axis direction on the section and gradually decreases from the slope top to the bottom. Due to the compression of the slope into the pit, a large sliding trend forms, resulting in tension failure of the pit's bottom and displacement along the positive direction of the z-axis. Meanwhile, the tensile crack at the rear edge of the slope decreases at the slope top, and the displacement gradually

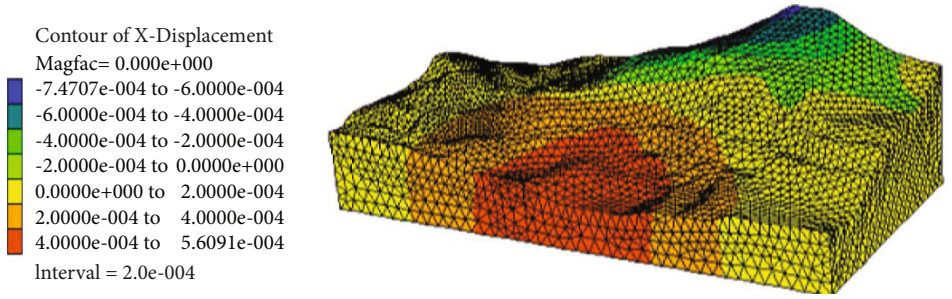

(a) The displacement cloud chart of the X direction

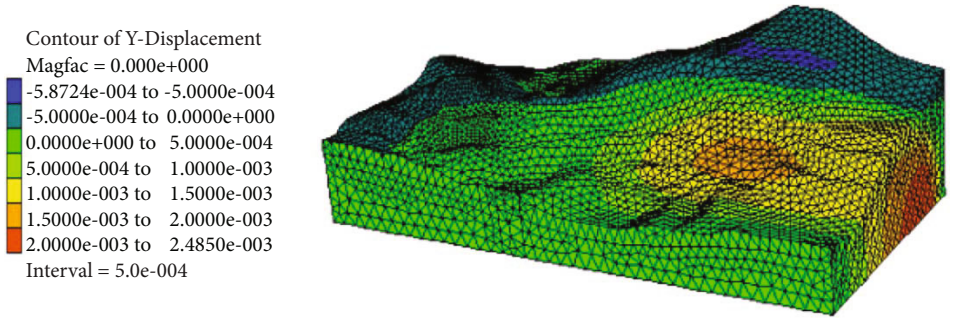

(b) The displacement cloud chart of the Y direction

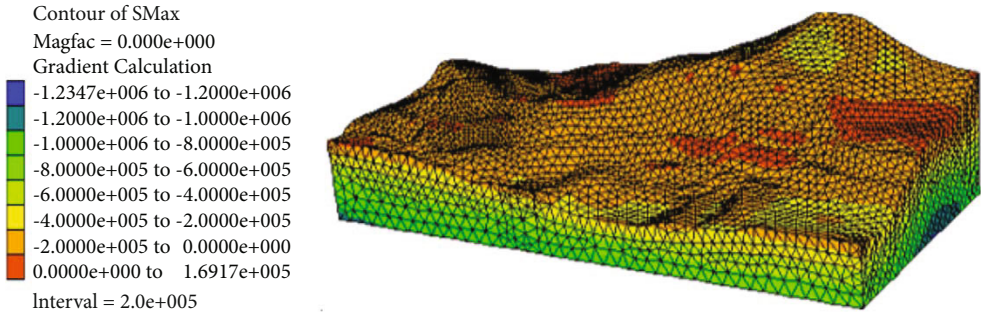

(c) The displacement cloud chart of the Z direction

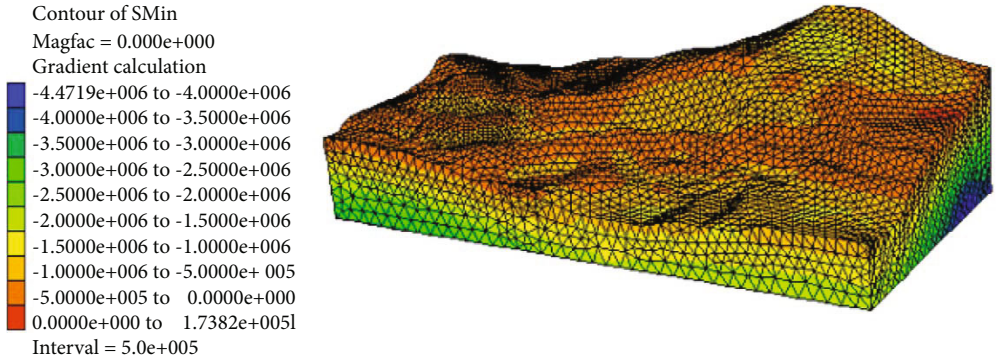

(d) The cloud diagram of the plastic belt

Figure 12: Displacement cloud chart and plastic zone of slope.

decreases. The displacement in the X direction of both sides of the slope is small, and the displacement in the x direction of the middle main slope is obviously less than that in the Y direction; the displacement is mainly produced in the direction of the y-axis outside the north side slope, which is consistent with the displacement of landslides along the main axis. Due to the extrusion of the slope into the pit, the rock mass at the bottom of the pit shows a large sliding trend, which causes the uplift of the bottom of the pit to form tensile failure, and the trailing edge of the slope pulls down cracks and generates positive displacement. The displacement distribution in the z direction of the slope is generally consistent with the overall displacement distribution. The surface displacement

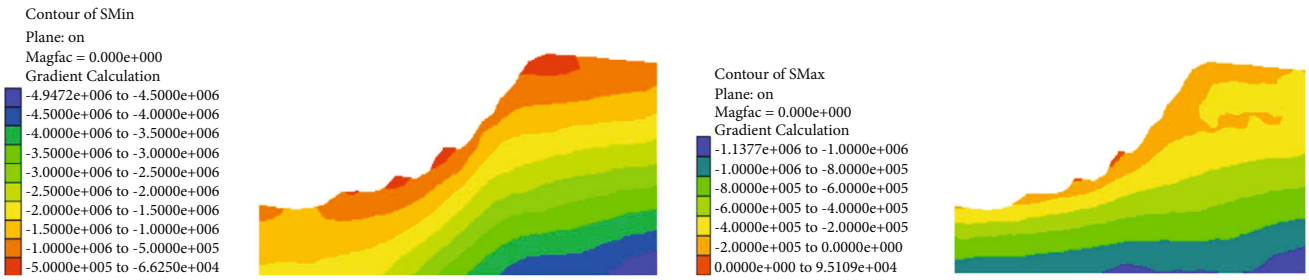

Figure 13: Cloud chart of the maximum and minimum principal stress of $x = 350$ section.

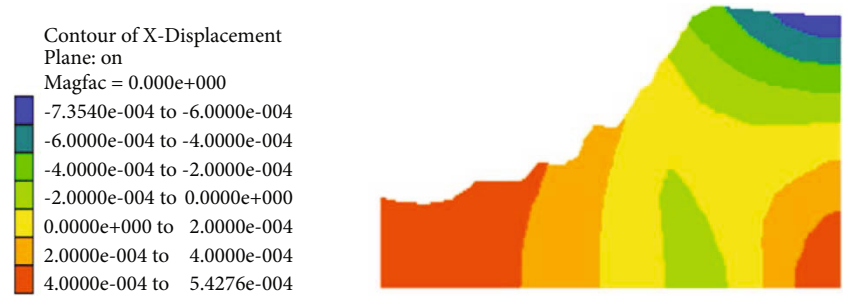

(a) Displacement cloud chart of $x = 350$ section in the X direction

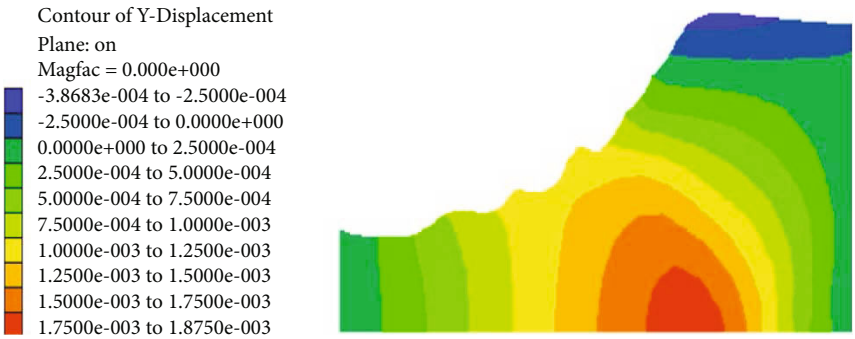

(b) Displacement cloud chart of $x = 350$ section in the Y direction

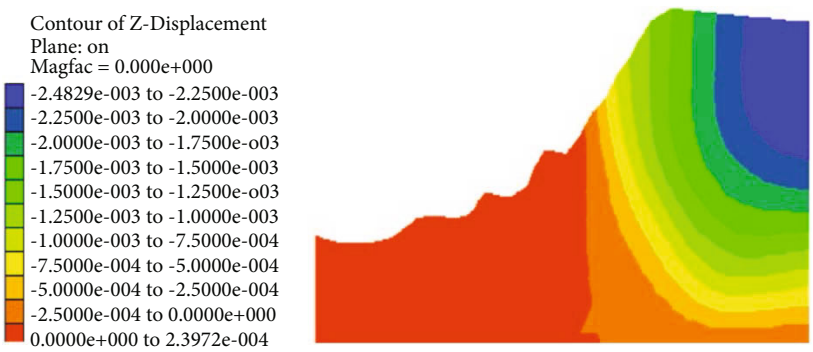

(c) Displacement cloud chart of $x = 350$ section in the Z direction

Figure 14: Displacement cloud chart of $x = 350$ section of the slope.

variation is the largest, and the downward displacement value decreases gradually.

6. Conclusion

In this study, the rock slope of an open-pit mine was taken as the research object. The physical parameters of each rock layer were obtained by means of field geological exploration, engineering drilling, geophysical exploration, and large-scale direct shear tests. The seepage deformation and failure were analyzed using GEOSLOPE, and a three-dimensional numerical simulation of the slope was carried out using FLAC^{3D}. The following conclusions are obtained:

(1) The 1~3 observation points have consistent slope inclination values and a steep dip angle that is close to the slope angle and slightly larger than the angle of the slope toe of the dominant structural plane; the intersection inclination of the two groups of structural planes at observation point 4 is consistent with the slope inclination. The angle between the intersection inclination of the structural planes and the slope inclination is less than 45°, and the intersection inclination angle is less than the slope inclination angle, but the intersection inclination angle is 10.3°, which is less than the joint fracture friction angle of 16.3°. The slope basically has a stable structure

(2) The Janbu method was used to calculate and analyze the seepage stability of the slope. Under the action of rainfall seepage, the safety factor of the 1-1 section decreases, but it is in a stable state. The safety factor of the 4-4 section is less than the minimum safety factor under three working conditions, making it a dangerous area. There is a possibility of overall sliding failure occurring on the slope platform

(3) The maximum principal stress area is mainly vertical self-weight stress that is distributed in the lower part of the slope, and the minimum principal stress area corresponds to the free surface of the slope. Due to the dense development of random structural surfaces, the local stress is released in the free direction, and a reverse tensile stress area appears, which is consistent with the failure phenomenon of the toppling tensile fracture caused by the development of the random structural surface of the slope

Data Availability

The data used to support the findings of this study are included within the article, and further data or information required is available from the corresponding author upon request.

Conflicts of Interest

The authors declare no conflicts of interest.

Acknowledgments

This project was supported by the Science and Technology Plan of Liaoning Province (2020JH2/10300100) and the Special Project of Guiding Local Scientific and Technological Development by the Central Government of Liaoning Province (2021JH6/10500015).

References

[1] L. Xie, J. Zhang, Y. Qin, J. Wang, W. Qiao, and J. Qian, "Displacement evolution of reverse-dip rock slope considering the change of the reservoir level," *Environmental Earth Sciences*, vol. 80, no. 21, article 10004, 2021.

[2] Z. Tao, C. Zhu, M. He, and M. Karakus, "A physical modeling-based study on the control mechanisms of negative Poisson's ratio anchor cable on the stratified toppling deformation of anti-inclined slopes," *International Journal of Rock Mechanics and Mining Sciences*, vol. 138, article S1365160921000204, p. 104632, 2021.

[3] C. Mu, X. Y. Yu, B. C. Zhao, D. D. Zhang, X. W. Mao, and J. Zhu, "The formation mechanism of surface landslide disasters in the mining area under different slope angles," *Advances In Civil Engineering*, vol. 2021, Article ID 6697790, 13 pages, 2021.

[4] Y. L. Zhai, P. Y. Yang, and L. Li, "Analytical solutions for the design of shotcreted waste rock barricades to retain slurried paste backfill," *Construction and Building Materials*, vol. 307, article S0950061821023813, p. 124626, 2021.

[5] C. Zhu, M. Karakus, M. He et al., "Volumetric deformation and damage evolution of Tibet interbedded skarn under multistage constant-amplitude-cyclic loading," *International Journal of Rock Mechanics and Mining Sciences*, vol. 152, article S136516092200034X, p. 105066, 2022.

[6] L. Yuan, C. Li, S. Li et al., "Mine slope stability based on fusion technology of InSAR monitoring and numerical simulation," *Scientific Programming*, vol. 2022, 8643510 pages, 2022.

[7] D. H. Chen, H. E. Chen, W. Zhang, J. Q. Lou, and B. Shan, "An analytical solution of equivalent elastic modulus considering confining stress and its variables sensitivity analysis for fractured rock masses," *Journal of Rock Mechanics and Geotechnical Engineering*, vol. 14, no. 3, article S1674775521001360, pp. 825–836, 2022.

[8] Y. Xue, J. Liu, P. G. Ranjith, Z. Zhang, F. Gao, and S. Wang, "Experimental investigation on the nonlinear characteristics of energy evolution and failure characteristics of coal under different gas pressures," *Bulletin of Engineering Geology and the Environment*, vol. 81, p. 38, 2022.

[9] Y. Xue, J. Liu, X. Liang, S. Wang, and Z. Ma, "Ecological risk assessment of soil and water loss by thermal enhanced methane recovery: numerical study using two-phase flow simulation," *Journal of Cleaner Production*, vol. 334, p. 130183, 2022.

[10] F. Q. Wu, J. Wu, H. Bao, B. Li, Z. G. Shan, and D. H. Kong, "Advances in statistical mechanics of rock masses and its engineering applications," *Journal of Rock Mechanics and Geotechnical Engineering*, vol. 13, no. 1, article S1674775520301669, pp. 22–45, 2021.

[11] D. Cambio, D. D. Hicks, K. Moffitt, M. Yetisir, and J. L. Carvalho, "Back-analysis of the Bingham Canyon South Wall: a quasi-static complex slope movement mechanism," *Rock Mechanics and Rock Engineering*, vol. 52, no. 12, article 1958, pp. 4953–4977, 2019.

[12] Z. Q. Yang, X. L. Fan, Y. Yang et al., "Deformation patterns and failure mechanism of high and steep stratified rock slopes with upper steep and lower gentle style induced by step-by-step excavations," *Environmental Earth Sciences*, vol. 81, no. 8, article 10327, 2022.

[13] S. Srikrishnan, J. L. Porathur, and H. Agarwal, "Impact of earthquake on mining slopes-a numerical approach," *Arabian Journal of Geosciences*, vol. 7, no. 12, article 1144, pp. 5193–5208, 2014.

[14] F. Y. Chen and W. G. Zhang, "Influence of spatial variability on the uniaxial compressive responses of rock pillar based on 3D random field," *Asce-Asme Journal Of Risk And Uncertainty In Engineering Systems Part A-Civil Engineering*, vol. 7, no. 3, 2021.

[15] B. Cao, S. Wang, D. Q. Song, H. Du, and W. Q. Guo, "Investigation on the deformation law of inner waste dump slope in an open-pit coal mine: a case study in Southeast Inner Mongolia of China," *Advances In Civil Engineering*, vol. 2021, Article ID 9953554, 18 pages, 2021.

[16] Z. H. Li, Y. J. Jiang, Z. G. Tao, and M. C. He, "Monitoring prediction of a rockslide in an open-pit mine and numerical analysis using a material instability criterion," *Bulletin of Engineering Geology and the Environment*, vol. 78, no. 3, article 1224, pp. 2041–2053, 2019.

[17] K. Zhang, X. J. Yang, X. B. Cui, Y. Wang, and Z. G. Tao, "Numerical simulation analysis of NPR anchorage monitoring of bedding rock landslide in open-pit mine," *Advances In Civil Engineering*, vol. 2020, Article ID 8241509, 17 pages, 2020.

[18] G. Y. Xu and C. B. Yan, "Numerical simulation for influence of excavation and blasting vibration on stability of mined-out area," *Journal of Central South University of Technology*, vol. 13, no. 5, article 91, pp. 577–583, 2006.

[19] B. Li, Z. Feng, G. Z. Wang, and W. P. Wang, "Processes and behaviors of block topple avalanches resulting from carbonate slope failures due to underground mining," *Environmental Earth Sciences*, vol. 75, no. 8, article 5529, 2016.

[20] Z. G. Tao, Z. Chun, M. C. He, and K. M. Liu, "Research on the safe mining depth of anti-dip bedding slope in Changshanhao mine," *Geomechanics And Geophysics For Geo-Energy And Geo-Resources*, vol. 6, no. 2, article 159, 2020.

[21] W. X. Zhu, H. W. Jing, L. J. Yang, B. Pan, and H. J. Su, "Strength and deformation behaviors of bedded rock mass under bolt reinforcement," *International Journal of Mining Science and Technology*, vol. 28, no. 4, article S2095268617305414, pp. 593–599, 2018.

[22] Z. Y. Liang, L. Liang, Y. Z. Cai, and A. Bertoni, "The influence factors of the stability of tailings dam based on multi-source information fusion method," *Journal Of Intelligent & Fuzzy Systems*, vol. 37, no. 3, pp. 3365–3372, 2019.

[23] C. G. Gong, S. G. Lei, Z. F. Bian, Y. Liu, Z. Zhang, and W. Cheng, "Analysis of the development of an erosion gully in an open-pit coal mine dump during a winter freeze-thaw cycle by using low-cost UAVs," *Remote Sensing*, vol. 11, no. 11, article rs11111356, p. 1356, 2019.

[24] L. Zhao and G. You, "Rainfall affected stability analysis of Maddingley Brown coal eastern batter using Plaxis 3D," *Arabian Journal of Geosciences*, vol. 13, no. 20, article 6038, 2020.

[25] Q. Yin, J. Wu, Z. Jiang et al., "Investigating the effect of water quenching cycles on mechanical behaviors for granites after conventional triaxial compression," *Geomechanics and Geophysics for Geo-Energy and Geo-Resources*, vol. 8, no. 2, article 388, 2022.

[26] G. Li, Y. Hu, S. M. Tian, and H. L. Huang, "Analysis of deformation control mechanism of prestressed anchor on jointed soft rock in large cross-section tunnel," *Bulletin of Engineering Geology and the Environment*, vol. 80, no. 12, article 2470, pp. 9089–9103, 2021.

[27] Z. Dou, Y. Liu, X. Zhang et al., "Influence of layer transition zone on rainfall-induced instability of multilayered slope," *Lithosphere*, vol. 2021, no. Special 4, 2021.

[28] Z. Dou, S. Tang, X. Zhang et al., "Influence of shear displacement on fluid flow and solute transport in a 3D rough fracture," *Lithosphere*, vol. 2021, no. Special 4, 2021.

[29] Y. Q. Su, F. Q. Gong, S. Luo, and Z. X. Liu, "Experimental study on energy storage and dissipation characteristics of granite under two-dimensional compression with constant confining pressure," *Journal of Central South University*, vol. 28, no. 3, article 4649, pp. 848–865, 2021.

[30] X. Wang, J. Li, X. Zhao, and Y. Liang, "Propagation characteristics and prediction of blast-induced vibration on closely spaced rock tunnels," *Tunnelling and Underground Space Technology*, vol. 123, article S0886779822000566, p. 104416, 2022.

[31] Y. Ye, Z. H. A. N. G. Guangcheng, C. H. E. N. Hongjie, W. Mingfei, B. Liulei, and C. Zheng, "Study on the failure mechanism of rock slope with layered cataclastic structure," *Chinese Journal of Rock Mechanics and Engineering*, vol. 40, pp. 365–381, 2021.